The International Journal of Advanced Manufacturing Technology (2021) 116:1843–1854
https://doi.org/10.1007/s00170-021-07564-8

ORIGINAL ARTICLE

The effect of superimposed ultrasonic vibration on tensile behavior of 6061-T6 aluminum alloy

Bangfu Wu[1] · Yang Cao[1] · Junshuai Zhao[1] · Wenfeng Ding[1]

Received: 10 February 2021 / Accepted: 27 June 2021 / Published online: 5 July 2021

Abstract

Ultrasonic vibration has been widely utilized in the forming and processing of metallic materials due to its advantages of reducing forming force and improving deformation ability and surface quality. However, the effect of ultrasonic vibration on the deformation mechanism of metallic material is still unclear. Based on the method of segmented resonant design, an ultrasonic vibration tensile device was developed, and its vibration performance was evaluated in this work. Furthermore, the ultrasonic vibration tensile tests were carried out to investigate the influence of ultrasonic vibration parameters on the properties of the 6061-T6 Al material. The results showed that the design error of 3.3% and ultrasonic vibration amplitude of 8.7 μm were achieved. Ultrasonic vibration reduced the stress required for 6061-T6 Al material deformation, but did not change Young's modulus and strain hardening rate. The stress reduction was proportional to the square of the ultrasonic vibration amplitude, indicating that ultrasonic softening was attributed to the changed dislocation of 6061-T6 Al material. Meanwhile, the ultrasonic vibration has no permanent effects on the tensile behavior of 6061-T6 Al material.

Keywords Ultrasonic vibration · Tensile behavior · Stress-strain · Aluminum alloy · Acoustic softening

1 Introduction

In 1955, Blaha and Langenecker superimposed ultrasonic vibration on the tensile test of Zinc single crystal and found that the material flow stress was reduced significantly by the ultrasonic vibration, which was called the "Blaha effect" [1]. Subsequently, many researchers have revealed some similar results (i.e., reduction of flow stress, improvement of deformation ability and surface quality) when ultrasonic vibration was applied in the deformation or processing of metal materials. Recently, the "Blaha effect" has been widely utilized in the different deformation processes of metallic materials, such as extrusion [2, 3], wire drawing [4, 5], upsetting [6], and grinding [7, 8].

To understand the underlying mechanism of material deformation with applied ultrasonic vibration, many scholars made enormous efforts and proposed some mechanisms such as acoustic softening [9], acoustic hardening [10], stress superposition [11], and reduction of friction coefficient [12]. The above-mentioned mechanisms could be divided into volume effect and surface effect [13, 14]. The volume effect declared that ultrasonic vibration changed the intrinsic properties of metallic materials, which led to the decrease of flow stress. And the surface effect indicated that the decrease of flow stress was attributed to relative motion characteristics of the tool and workpiece caused by ultrasonic vibration. At present, plenty of works mainly focus on the ultrasonic motion characteristics and the surface effect is confirmed by experiments, but the volume effect is still unclear. Therefore, it is necessary to study the deformation characteristics of materials under the ultrasonic vibration.

Ultrasonic vibration tensile test could eliminate the interference of surface effect, which has become an effective approach to investigate mechanical properties and deformation behavior of the material during ultrasonic vibration. Daud et al. [15] carried out ultrasonic vibration tensile experiments and finite element simulation to predict the stress-strain relationship of aluminum alloy. Results showed that stress superposition was not enough to explain the influence of ultrasonic vibration on the metal forming process. Zhong [16] investigated the effect of ultrasonic vibration on the tensile behavior

✉ Wenfeng Ding
dingwf2000@vip.163.com

[1] National Key Laboratory of Science and Technology on Helicopter Transmission, Nanjing University of Aeronautics and Astronautics, Nanjing 210016, China

of 6063 aluminum alloy. It was concluded that acoustic softening and stress superposition led to the reduction of flow stress of the material. Gu [17] found that the acoustic softening and acoustic hardening existed simultaneously during the tensile deformation of T2 copper. Gao et al. [18] conducted an ultrasonic vibration tensile test of TC1 titanium alloy and pointed out that ultrasonic vibration could significantly reduce the yield strength and tensile strength of the material, but the mechanism of the ultrasonic effect was not discussed in detail. Wen et al. [19] claimed that there was an ultrasonic energy threshold in the plastic deformation process of AZ31. Namely, the acoustic softening was the dominant mechanism in low energy and the acoustic hardening was the dominant mechanism in high energy. Dutta et al. [20] investigated the effect of transverse ultrasonic vibration on the microstructure of low-carbon steel during the tensile process. It was found that acoustic softening was associated with the reduced sub-grain formation of the material.

In addition, Jiang et al. [21] performed a series of ultrasonic vibration tensile experiments of titanium foil and found that the reduction of flow stress was inversely proportional to the applied time of ultrasonic vibration. Xiang et al. [22] demonstrated that the reduction of flow stress was mainly affected by the stress superposition, acoustic softening, and Hall-Petch strengthening when superimposing ultrasonic vibration in the tensile process of high-volume fraction SiC_p/Al. Wang et al. [23] applied ultrasonic vibration to 5052 aluminum alloy during the tensile process, in which not only acoustic softening was found at the moment of the applied vibration, but also residual acoustic softening was observed when the vibration stopped. Mao et al. [24] carried out the ultrasonic vibration tensile test with the three kinds of aluminum samples to investigate the mechanism of acoustic softening. It was concluded that acoustic softening was attributed to the interactions between the dislocations activated by ultrasonic vibration and precipitates. Although many studies analyzed the influence of ultrasonic vibration parameters on the deformation mechanism of materials, almost all of them were conducted with the ultrasonic amplitude measured in a no-load state. In the actual tensile process, the rather larger tensile load could reduce the actual vibration amplitude and further affect tensile performance, which was insufficiently considered in the above-mentioned studies. Moreover, the effect of ultrasonic vibration on the final material properties needed to be further studied.

Based on the method of segmented resonance design, an ultrasonic vibration tensile device was developed. The ultrasonic vibration amplitude real-time monitoring system was applied, and the vibration characteristics of the device were evaluated. A series of tensile experiments were performed to study the effect of ultrasonic vibration parameters on the tensile properties of 6061-T6 aluminum alloy. In addition, the underlying mechanism of acoustic softening was discussed.

2 Ultrasonic vibration tensile device

The ultrasonic vibration axial tensile system contains an electromechanical universal testing machine and ultrasonic vibration tensile device, as shown in Fig. 1. This configuration ensures that the propagation direction of the longitudinal acoustic wave is identical to the direction of tensile force. As depicted in Fig. 1 b, the ultrasonic vibration tensile device is composed of a support structure and an ultrasonic resonance system. The system includes a piezoelectric transducer, a front horn, a specimen, and a rear horn. They are assembled in the respective sequence by screwed connections. The support structure provides a fixed position for the ultrasonic resonance system to load the tensile force. The ultrasonic resonance system is developed to meet the requirement that the specimen vibrates at its natural frequency during the tensile test.

The piezoelectric transducer converts electric energy into ultrasonic mechanical vibration, then the front horn amplifies ultrasonic vibration and delivers it to the specimen, the rear horn receives the mechanical wave and reflects it, thus forming the stationary wave with multiple nodes and antinodes. In this case, the center of the specimen is located at the node position, and the maximum acoustic stress can be achieved. The commercial piezoelectric transducer can excite a mechanical sine vibration with a frequency of approximately 19.6 kHz. To ensure that the resonant frequency of the ultrasonic resonance system is consistent with the excitation frequency of the piezoelectric transducer, the method of segmented resonance design is introduced to calculate the geometry dimension of the front horn, specimen, and the rear horn respectively, where the resonant frequency of every part is 19.6 kHz, and the resonant length is half of the longitudinal wave of the used material.

2.1 The horn

During the ultrasonic vibration tensile process, the horn plays an important role in the performance of the ultrasonic vibration tensile device because it not only transmits the acoustic wave and amplifies the vibration amplitude but also builds a fixed connection between the specimen and the support structure. To eliminate the design error as much as possible, the front horn and rear horn have the same geometry. A composite conical horn, consisting of a cylindrical section and conical section, is adopted to improve a magnification factor M, as shown in Fig. 2. The resonant frequency equation of the composite conical horn can be calculated as [25]:

$$\tan(kx_1) = \tan\left(\tan^{-1}\left(\frac{N-1}{kx_2}\right) - kx_2\right) - \frac{N-1}{Nkx_2} \quad (1)$$

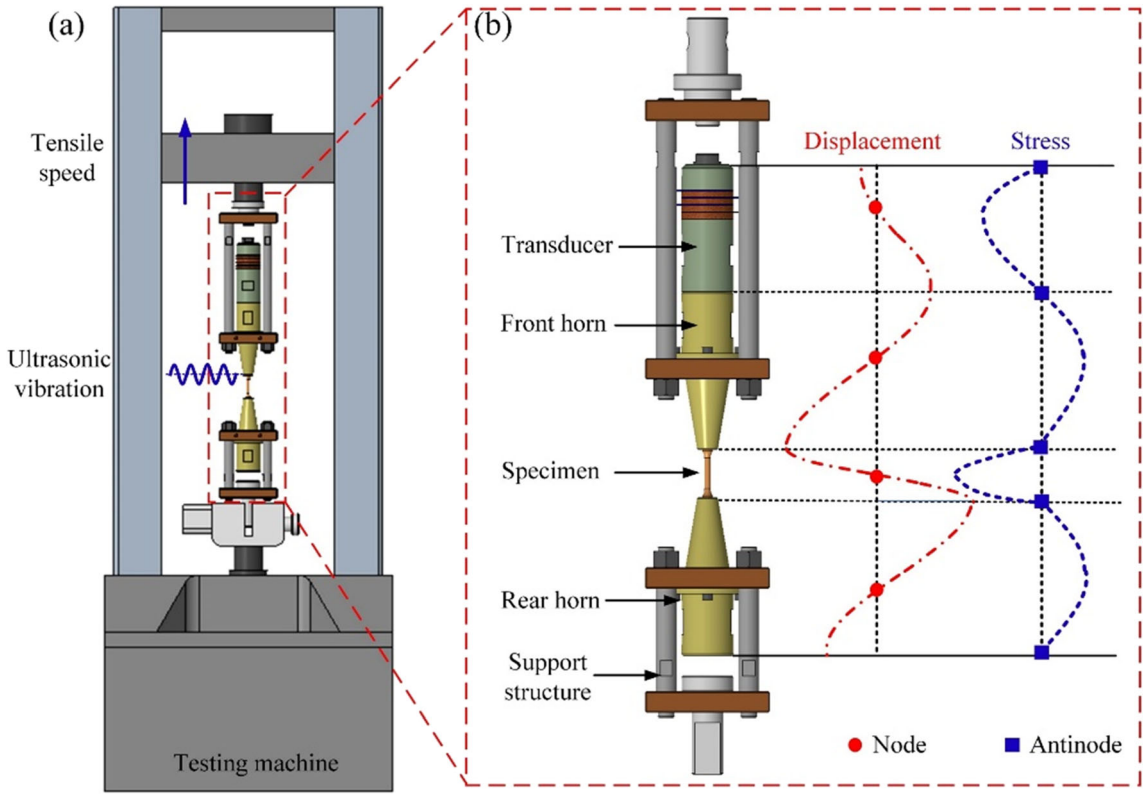

Fig. 1 Schematic of experiment setup: **a** electromechanical universal testing machine, **b** ultrasonic vibration tensile device

where k is the circular wavenumber, $k = 2\pi f/\sqrt{E/\rho}$, f is the resonant frequency, E and ρ are the elastic modulus and density of materials respectively. N is the ratio of r_1 to r_2.

The magnification factor M of the composite conical horn can be expressed as:

$$M = N\lfloor \cos(kx_2) - \left(\tan(kx_1) + \frac{N-1}{N}\,\frac{1}{kx_2}\right).\sin(kx_2)\rfloor \quad (2)$$

2.2 The specimen

The specimen shape used in the tensile test is shown in Fig. 3. The geometry of the specimen is a dumbbell profile with a circular cross section, which is similar to conventional specimens. But the length of the specimen must be designed appropriately to have the same resonant frequency as the piezoelectric transducer. By integrating the dynamic equation of one-dimensional longitudinal wave in bars with the specific boundary conditions, the resonant frequency equation of the specimen is determined as follows [26]:

$$\begin{cases} \tan(kx_5) = \dfrac{a_3\sin(kx_3) + a_4\cos(kx_3)}{a_3\sin(kx_3) + a_4\cos(kx_3)} \\ a_1 = \cosh(\beta x_4) \\ a_2 = k\,\sin(\beta x_4)/\beta \\ a_3 = \cosh(\beta x_4)[\beta tanh(\beta x_4) - a\,\tanh(ax_4)]/k \\ a_4 = \sinh(\beta x_4)[\beta tanh(\beta x_4) - a\,\tanh(ax_4)]/k \end{cases} \quad (3)$$

where the constant $a = cosh^{-1}(r_5/r_3)/x_4$ and $\beta = \sqrt{a^2 + k^2}$.

According to GB/T 228-2002 standard (equivalent to ISO 6892:1998), the gauge length of the specimen is defined by:

$$x_3 = 5r_3 \quad (4)$$

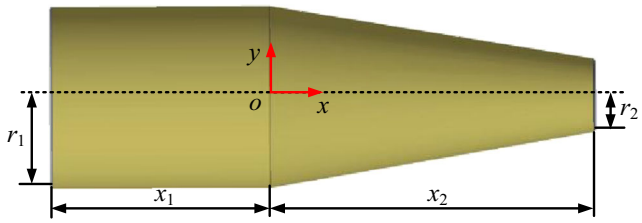

Fig. 2 Geometry of the composite conical horn

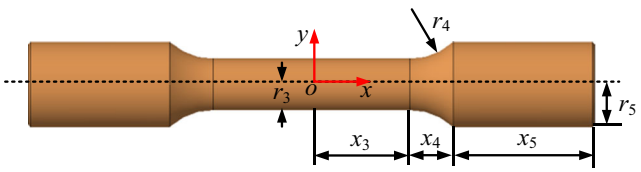

Fig. 3 Geometry of the specimen

Table 1 Material properties

Element	Material	Density ρ	Elastic modulus E	Poisson's ratio v
Horn	316 L	7930 kg/m^3	200 GPa	0.29
Specimen	6061-T6 Al	2770 kg/m^3	71 GPa	0.33

The radius and length of the arc transition section of the specimen can be calculated as follows [27]:

$$r_4 = \frac{(r_5-r_3)\sqrt{r_5^2-r_3^2}\ cosh^{-1}(r_5/r_3)-(r_5-r_3)^2}{\sqrt{r_5^2-r_3^2}\ cosh^{-1}(r_5/r_3)-2(r_5-r_3)} \tag{5}$$

$$x_4=\sqrt{\frac{(r_5-r_3)^2\sqrt{r_5^2-r_3^2}\ \cosh^{-1}(r_5/r_3)}{\sqrt{r_5^2-r_3^2}\ \cosh^{-1}(r_5/r_3)-2(r_5-r_3)}} \tag{6}$$

2.3 Ultrasonic resonance system

Modal is the natural vibration characteristics of a mechanical structure or part. Each model has a specific resonant frequency and vibration mode, which can be analyzed by the finite element method (FEM). In this work, FEM can not only verify the accuracy of the theoretical method about the horn and specimen but also analyze the vibration characteristics of the ultrasonic resonance system, thus reducing the design error and cost of the device.

The materials used for the horn and specimen are 316 L stainless steel (316 L) and 6061-T6 Aluminum alloy (6061-T6 Al) respectively. Their properties and chemical composition are listed in Tables 1 and 2. It is defined that r_1 = 25 mm, r_2 = 10 mm, r_3 = 3 mm, and r_5 = 5 mm. According to the Eqs. (1–6), the geometry dimensions of the horn and specimen are calculated and their longitudinal resonant modes are obtained, as shown in Fig. 4. As can be seen from Fig. 4 c and d, the resonant frequencies of the horn and specimen are 19275 Hz and 19543 Hz, respectively. Little error exists between the simulated and theoretical values (f = 19600 Hz), which verifies the feasibility of the theoretical method. However, the geometry dimensions of the horn need to be further modified by FEM to reduce the design error.

The mass reduction method is one of the effective methods to modify the mode of structure [28]. In particular, the screwed connection is applied between the horn and specimen, so the longitudinal resonant mode of the horn can be changed by setting a circular hole, which is located at the end of the horn. Figure 5 displays the effect of the length of hole h_1 on the resonant frequency of the horn, where the diameter of hole d_1 = 10 mm. The resonant frequency of the horn increases quickly from 19369 to 19734 Hz when the length of the hole varies from 5 to 30 mm. Furthermore, when h_1 = 20 mm, the resonant frequency of the horn is 19617 Hz, which has a small error with the design frequency.

The flange is used to fix the horn and transfer the external load during the tensile test. Although the flange is located at a node position, it inevitably leads to the drift of the resonant frequency of the horn. The frequency drift can be controlled by carefully designing the dimension of the flange. The thickness h_2 and diameter d_2 of the flange are optimized by FEM, as shown in Fig. 6. The smaller frequency drift and the larger stiffness are achieved by choosing the thickness h_2 = 7 mm and diameter d_2 = 70 mm, where the resonant frequency of the horn with flange is 19650 Hz.

For further improving the accuracy of the design process, it is necessary to obtain the vibration characteristics of the ultrasonic resonant system. According to the actual dimensions and material properties from manufacturers, all components of the piezoelectric transducer are initially modeled. Then the transducer, horn, and specimen are assembled to become an ultrasonic resonance system. The modal analysis of the ultrasonic resonance system is performed, and the longitudinal resonant mode is acquired, as illustrated in Fig. 7. The longitudinal resonant frequency of the ultrasonic resonance system is 19671 Hz, which is consistent with the theoretical frequency. With the known resonant frequency, the harmonic response of the ultrasonic resonance system is created. A displacement of 10 μm is imposed at the interface between the transducer and the horn. The relative vibration displacement and stress of the ultrasonic resonant system along the specimen axis are presented in Fig. 7. Obviously, the center displacement of the specimen equals zero and its stress value is the largest, which satisfies the design requirement.

Table 2 Chemical compositions of materials (%wt)

Material	C	Si	Mn	P	S	Ni	Cr	Mo	Fe	Cu	Mg	Zn	Ti	Al
316L	0.06	0.2	3.2	0.028	0.03	10.03	16.3	2.0	Bal.	–	–	–	–	–
6061-T6 Al	–	0.59	0.11	–	–	–	0.24	–	0.12	0.24	1.02	0.07	0.03	Bal.

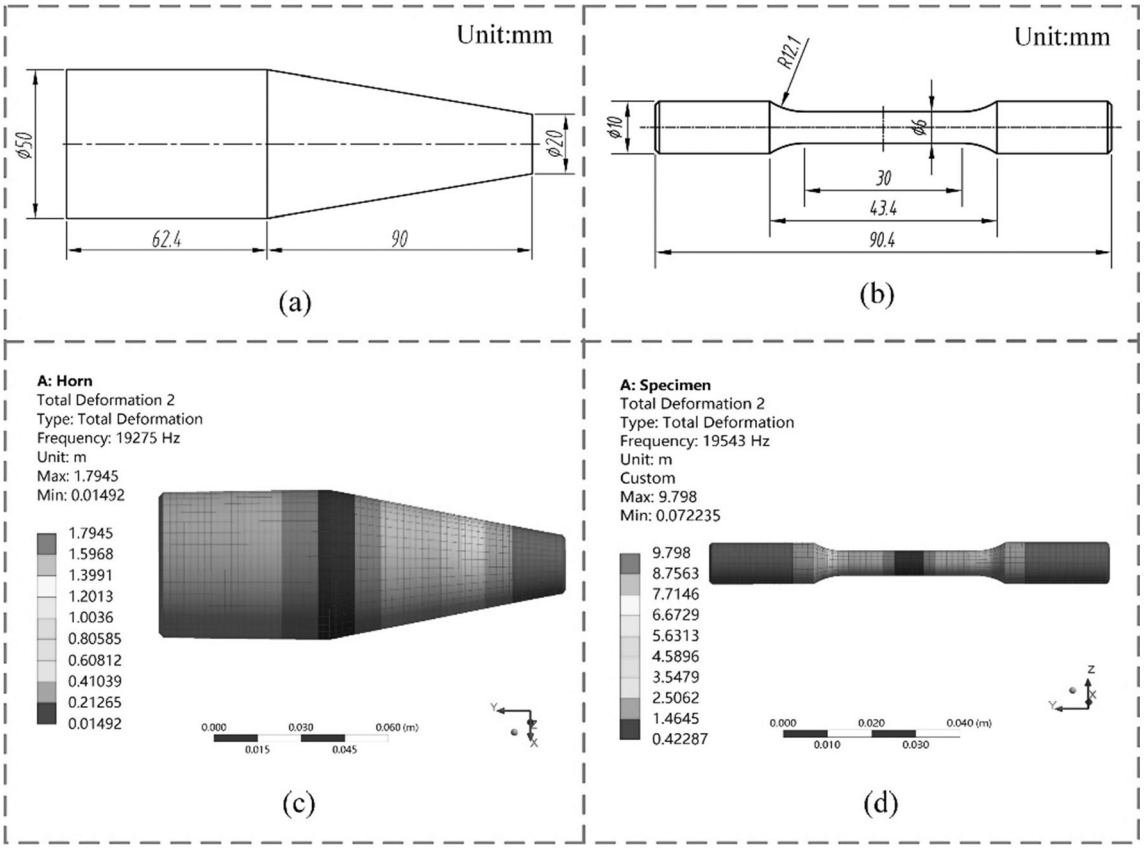

Fig. 4 Geometry dimensions and resonant mode for the horn and specimen

2.4 Vibration performance of ultrasonic vibration tensile device

On the basis of the designed results of Section 2.3, each part of the ultrasonic vibration tensile device is fabricated and assembled. The impedance test of the ultrasonic resonance system is performed using the PV502A impedance analyzer, as depicted in Fig. 8. The admittance chart and impedance-frequency curve are relatively regular. The dynamic resistance (R = 32.1 Ω) is at a low level, indicating that the energy dissipation of the ultrasonic resonance system is small, thus improving the converted efficiency between electric energy and acoustic energy. There is an error of 3.3% between the measured value (f = 19014 Hz) and the simulated value (f = 19671 Hz) of the resonance frequency. It is because that the actual material properties are different from the theoretical value during the design process.

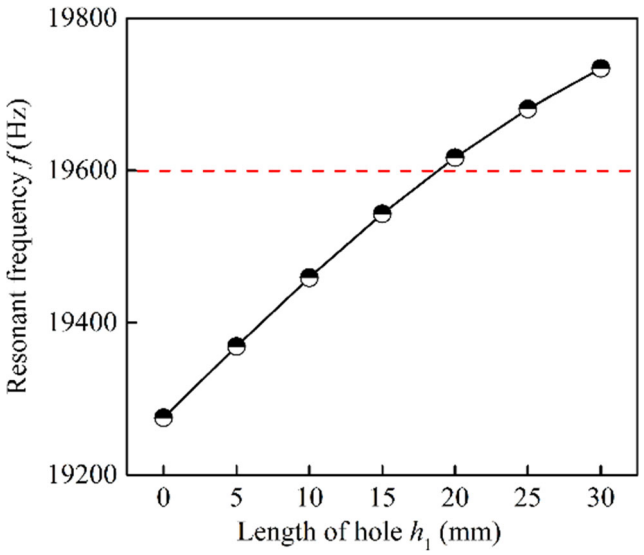

Fig. 5 The effect of length of the hole on the resonant frequency of the horn

Ultrasonic amplitude is an important parameter to evaluate the performance of ultrasonic vibration tensile device. The amplitude is measured by fixing the ultrasonic vibration tensile device on the electromechanical universal testing machine and the tensile load is applied to make each part of the device contact closely. Then output amplitude of the front horn is detected by an eddy current sensor (Micro-Epsilon EU05), as shown in Fig. 9. Ultrasonic vibration waveform is displayed by the oscilloscope and the peak of waveform corresponds to the ultrasonic amplitude. Different amplitudes can be obtained by changing the output power of the ultrasonic generator. When the output frequency of the ultrasonic generator increases from 18900 to19100 Hz, the standard sinusoidal

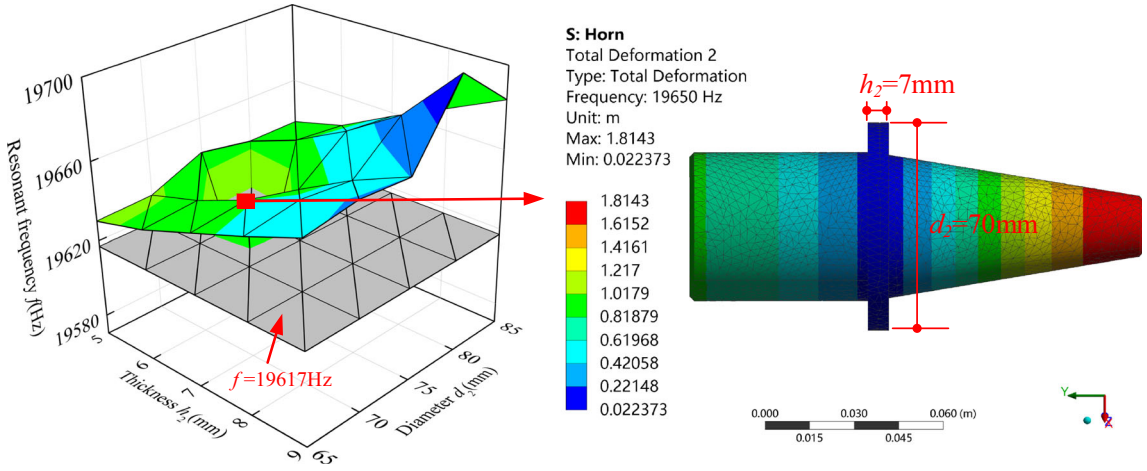

(a) (b)

Fig. 6 Optimization of the resonant frequency of horn: **a** the effect of flange dimensions on the resonant frequency, **b** optimized result

waveform can be observed on the oscilloscope, indicating that the device reaches a resonant state. Moreover, the amplitude increases linearly with the output power of the ultrasonic generator, and the maximum ultrasonic amplitude reaches 8.7 μm.

3 Experimental details

As mentioned above, the specimens were prepared with a gauge length of 30 mm. The tensile speed was fixed at 1 mm/min to allow that there is abundant time to apply ultrasonic vibration. To comprehensively understand the effect of ultrasonic vibration on the tensile properties of 6061-T6 Al, the ultrasonic vibration tensile tests were carried out with the different deformation stages, vibration time, and ultrasonic amplitudes. Details of the experiments are listed in Table 3 and the excitation frequency of the ultrasonic generator was 19000 Hz during the whole test.

The ultrasonic vibration was applied at the different deformation stages, as shown in Fig. 10. In test no.1, the conventional tensile process without superposing ultrasonic vibration was conducted to compare the ultrasonic vibration tensile test. To study the effect of duration time of pure ultrasonic vibration on the tensile behavior of the material, ultrasonic vibration was exerted to specimen before the tensile test no.2, and then the tensile process was similar to the conventional tensile test. During test no.4, it is difficult to determine the yield stage of 6061-T6 Al accurately, so ultrasonic vibration started to be imposed in the elastic stage, and then it was unloaded in the plastic deformation stage. The true stress-strain data was acquired from the measured software and the micromorphology of the fractured cross section was observed by a scanning electron microscope (COXEM EM30).

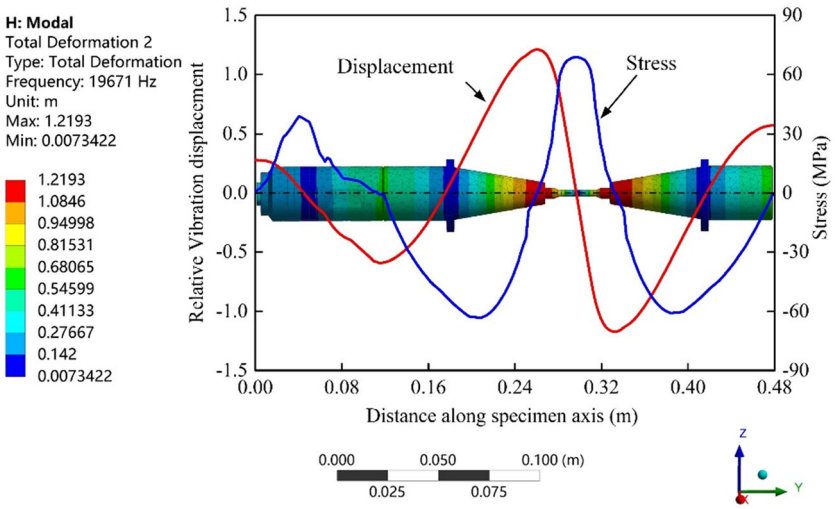

Fig. 7 Distribution of relative vibration displacement and stress of ultrasonic resonant system at longitudinal resonant mode

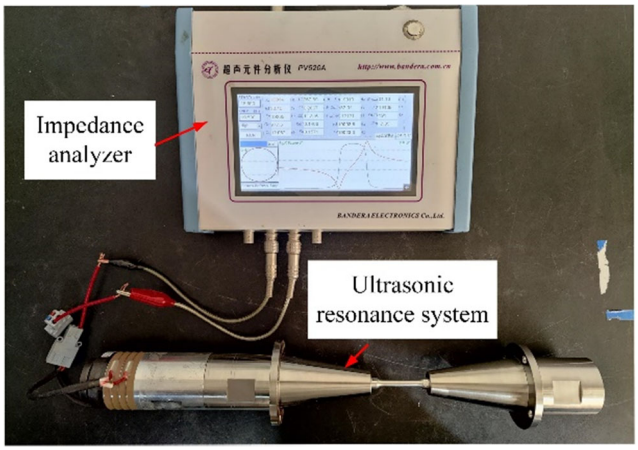

Fig. 8 Impedance test of the ultrasonic resonance system

4 Results and discussion

4.1 The effect of ultrasonic vibration on the different deformation stages

Figure 11 compares tensile stress-strain curves of 6061-T6 Al without and with ultrasonic vibration at different deformation stages. It can be seen from Fig. 11 a that the ultrasonic vibration is applied at the stress of 75 MPa and stopped with the stress of 265 MPa. During the deformation stage with ultrasonic vibration, the stress-strain curve is paralleled to that of conventional tensile, but the stress-strain curve diverges from the intrinsic trend. The slopes of the two stress-strain curves are 16991.5 and 16848.9, respectively, which indicates that ultrasonic vibration does not change Young's modulus of 6061-T6 Al material.

Figure 11 b shows the effect of ultrasonic vibration on the stress-strain curve of 6061-T6 Al during the yield stage. The ultrasonic vibration is applied as the specimen is still in the elastic stage and a similar trend of the stress-strain curve to Fig. 11 a is observed. Upon stopping the ultrasonic vibration in the plastic stage, the stress increases immediately to a certain value, and then, the stress-strain curve is consistent with the conventional tensile. It is interesting that the stress-strain curve with ultrasonic vibration is paralleled to but lower than that of the conventional tensile, indicating that ultrasonic vibration changes the deformation of the yield stage and reduces the yield strength of 6061-T6 Al.

Figure 11 c depicts the effect of ultrasonic vibration on the stress-strain curve of 6061-T6 Al during the plastic deformation stage. As soon as the ultrasonic vibration is applied, the stress value decreases rapidly by 10 MPa, then it gradually increases with the increase of strain. When the ultrasonic vibration is terminated, the stress increases quickly and then keeps a stable growth trend. During the duration of ultrasonic vibration, the reduction of stress is observed, which is attributed to acoustic softening. In addition, the paralleled stress-strain curves between the ultrasonic and conventional tensile test demonstrate that the strain hardening rate is not changed by the ultrasonic vibration. More importantly, the stress difference of position 1 (7.9 MPa) and position 2 (8.3 MPa) are basically equal, which indicates that there is no ultrasonic residual effect after stopping ultrasonic vibration.

4.2 The effect of ultrasonic vibration duration time on the tensile behavior

When the tensile specimen reached the resonant state, the maximum acoustic stress was generated in the middle position of the tensile specimen [29, 30]. It is assumed that the frequency of ultrasonic vibration is 20000 Hz, which means that the

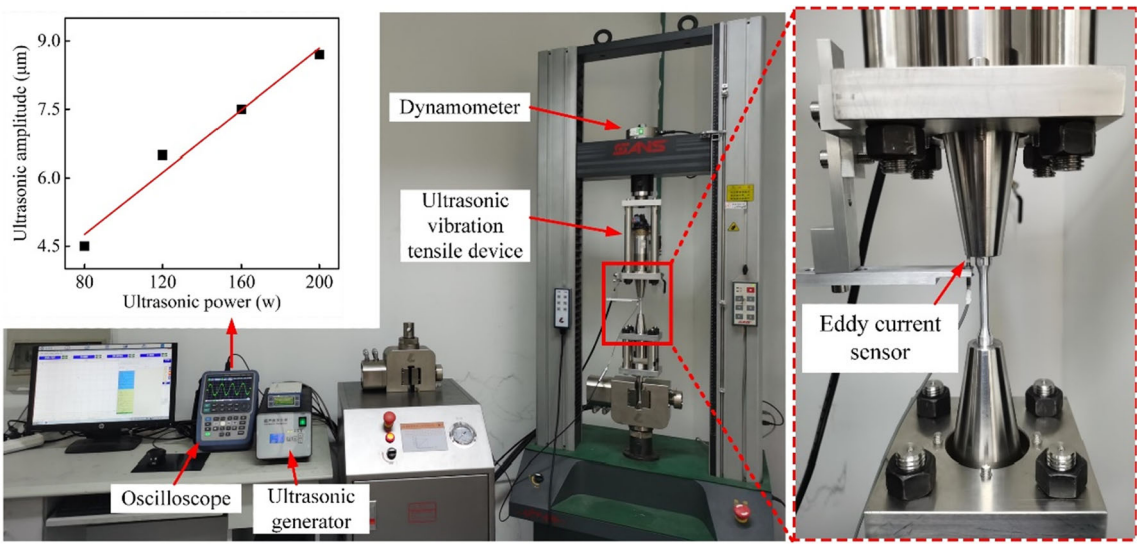

Fig. 9 Amplitude test of the ultrasonic vibration tensile device

Table 3 Experimental parameters

Test no.	Ultrasonic amplitude A (μm)	Applied ultrasonic vibration time t (s)
1	0	0
2	6.5	240
3	6.5	30
4	6.5	90
5	4.5	30
6	6.5	30
7	7.5	30
8	8.7	30

material is subjected to the alternated acoustic stress of 20,000 times per second, thus causing fatigue damage and failure of the material. Therefore, it is urgent to study the effect of ultrasonic vibration duration time on the mechanical properties of the material.

The stress-strain curve with the different ultrasonic vibration duration time before the tensile test is compared, as shown in Fig. 12. There was no apparent difference in the stress-strain curve of the duration time t= 0 s and t= 240 s before necking. While in the necking stage, the deviation of two curves is observed due to the uniform deformation of the material. It can be inferred that the alternating acoustic stress caused by ultrasonic vibration does not affect the tensile properties of 6061-T6 Al.

To further investigate the influence of ultrasonic vibration duration time on the material properties, the tensile strength σ_b and its corresponding elongation ε_b with the different number of cycles N ($N = ft$) are compared and displayed in Fig. 13. With the increase of the number of cycles, the tensile strength and elongation of the 6061-T6 Al material exhibit little difference. Under conditions of N = 0, the tensile strength is 337.5 MPa and the elongation of the material is 8.7%. When the number of cycles N increases to 4.56×10^6 (t = 240 s), the tensile strength and elongation of the material are 334.5 MPa and 8% respectively. It is demonstrated that the ultrasonic vibration has no permanent effect on the tensile properties of 6061-T6 Al materials at the tested levels.

4.3 The Effect of ultrasonic amplitude on the material deformation

Figure 14 presents the tensile stress-strain curves of 6061-T6 Al with the different ultrasonic amplitudes which are applied in the plastic stage. The stress reduction can be observed at the different ultrasonic amplitude levels. Specifically, the higher the ultrasonic amplitude, the larger the stress reduction, which indicates that acoustic softening is dependent on the ultrasonic amplitude. Similar results were reported by many researchers. Huang et al. [31] found that there has been a linear relationship between the stress reduction value and ultrasonic amplitude, and concluded that the ultrasonic energy was absorbed by the lattice imperfection, thus resulting in acoustic softening. However, Langenecker et al. [32] proposed that the stress reduction was proportional to the ultrasonic energy density. The above relation was attributed to the that the ultrasonic energy was preferentially absorbed by the dislocation line of the material, which lowered the energy barriers and accelerated the movement of dislocation, thus reducing the deformation stress. Based on the viewpoint from the dislocation theory proposed by Langenecker, Mao et al. [24] further summarized that the interaction between ultrasonic vibration and the precipitated strengthening phase was also one of the reasons for acoustic softening.

Ultrasonic energy density can be expressed as [33]:

$$E_u = \frac{1}{2}\rho c \omega^2 A^2 \tag{7}$$

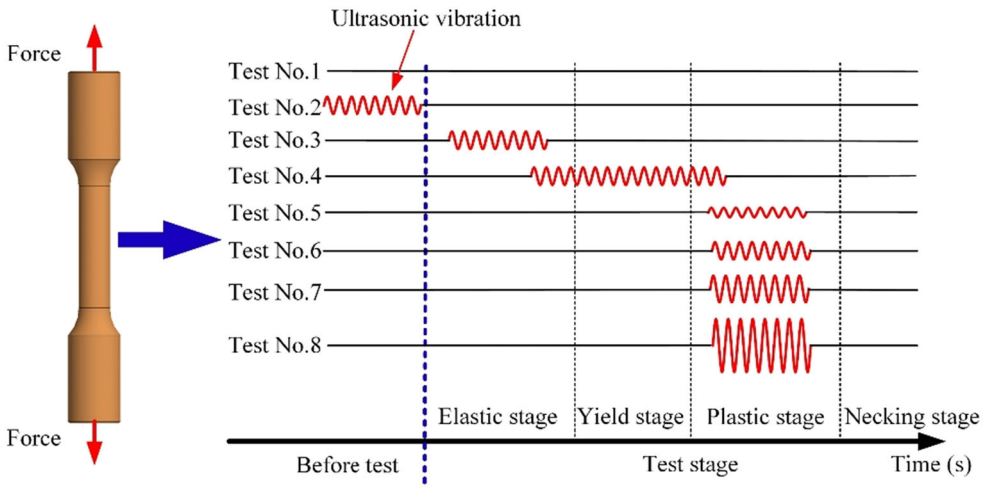

Fig. 10 The schematic diagram of the applied ultrasonic vibration in different deformation stages

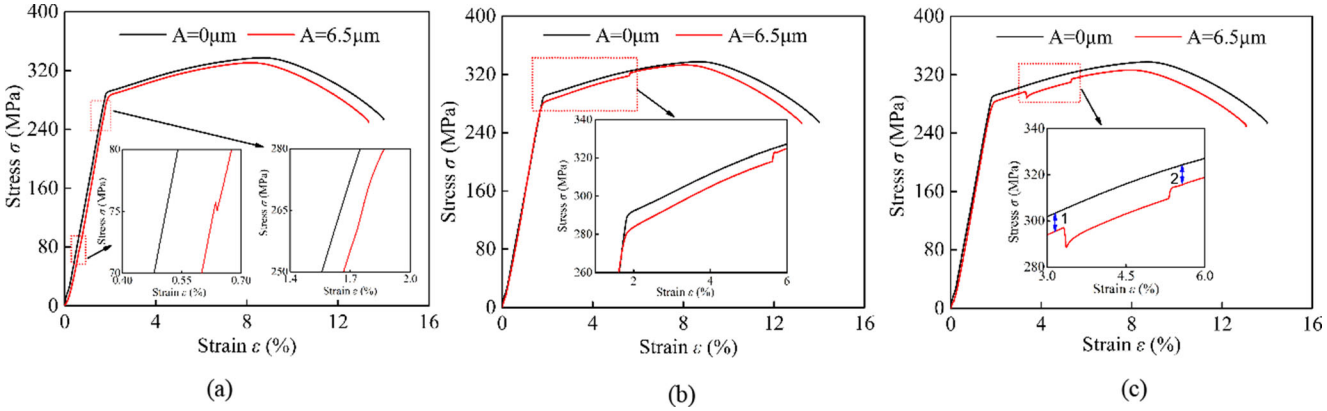

Fig. 11 The effect of ultrasonic vibration on the stress-strain at a elastic stage, b yield stage, and (c) plastic stage

where c is the acoustic velocity of material and ω is the angular frequency.

According to Eq. (7), it is known that the ultrasonic energy density is related to the material properties and ultrasonic parameters. As seen from the above analysis, there is a certain proportional relationship between the stress reduction $\triangle\sigma$ and the ultrasonic amplitude A^n (n = 1, 2) with the same material and ultrasonic frequency.

The stress reduction with the different ultrasonic amplitudes is displayed in Fig. 15. It is found that the stress reduction increases with the increase of ultrasonic amplitude. When the ultrasonic amplitude is 4.5 μm, the stress reduction is 3.3 MPa. As the ultrasonic amplitude increases to 8.7 μm, a stress reduction of 11.3 MPa is observed. The parameter fitting is carried out to obtain the relationship between the stress reduction and ultrasonic vibration amplitude. The stress reduction is proportional to the square of the ultrasonic amplitude, which was consistent with Langenecker's result. It can be inferred that the acoustic softening is the result of the changed dislocation of 6061-T6 Al alloy with the ultrasonic vibration.

As previously reported by Wen et al. [19], an energy threshold existed during the vibration plastic forming process of AZ31 magnesium alloy. When the ultrasonic vibration energy was lower than the energy threshold, the acoustic softening controlled the deformation mechanism. On the contrary, the material deformation was mainly affected by the acoustic hardening. These two mechanisms further affected the tensile strength, elongation, and other tensile properties of the material.

The difference of material and experimental error inevitably lead to the deviation of the stress-strain curve. In this case, the relative parameters of tensile properties of the material are defined to investigate the effect of ultrasonic amplitude on the tensile behavior of 6061-T6 Al. Figure 16 shows the relative tensile strength σ_{br}, relative tensile elongation ε_{br} and relative fracture elongation ε_{fr}, which can be expressed as follows:

$$\sigma_{br} = \sigma_b - \sigma_y \tag{8}$$

$$\varepsilon_{br} = \varepsilon_b - \varepsilon_y \tag{9}$$

$$\varepsilon_{fr} = \varepsilon_f - \varepsilon_y \tag{10}$$

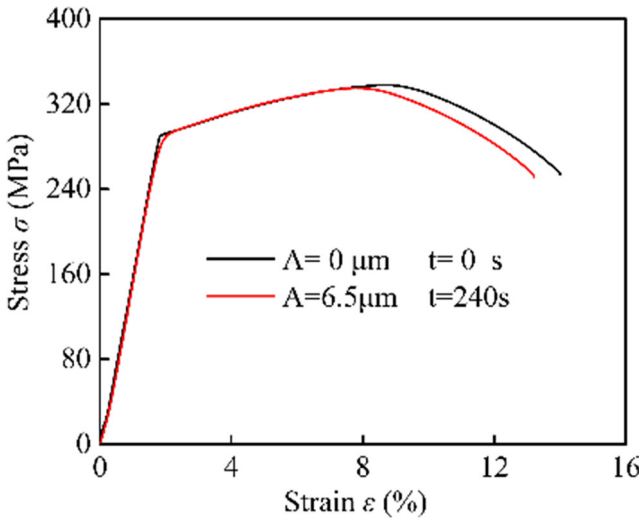

Fig. 12 Comparison of stress-strain curves with ultrasonic vibration duration time t=0 s and t=240 s before the tensile test

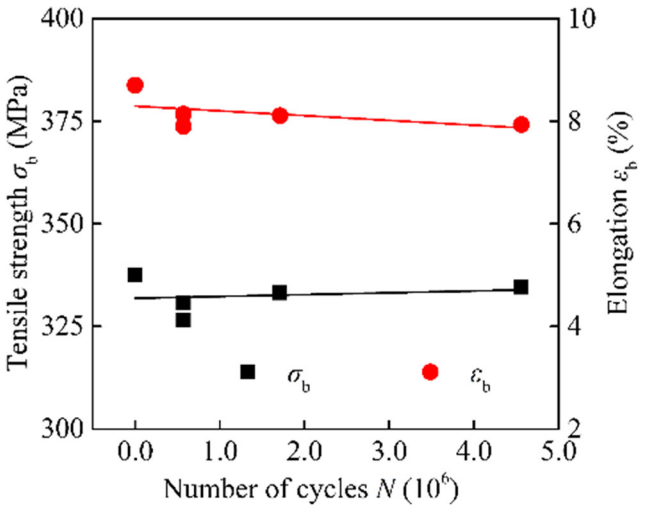

Fig. 13 The Effect of the number of cycles on the tensile strength and elongation

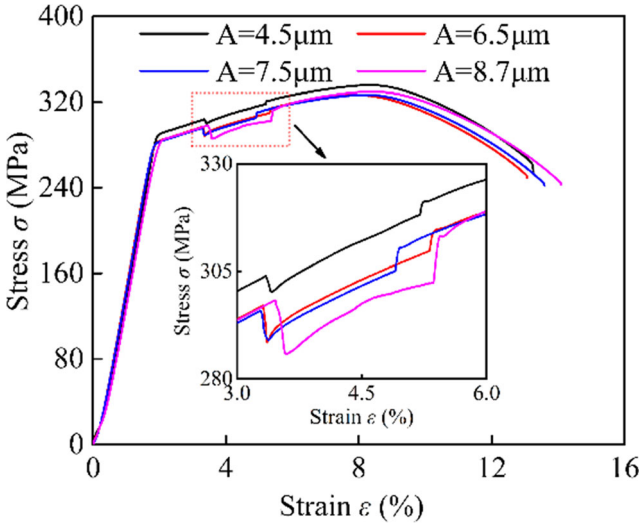

Fig. 14 Stress-strain curves under different ultrasonic amplitudes

where σ_y and ε_y are the strength and elongation at yield point, respectively. σ_b and ε_b are the strength and elongation at the ultimate tensile strength of the material, respectively. ε_f is the fractured elongation.

The influence of ultrasonic amplitude on the σ_{br}, ε_{br}, and ε_{fr} of 6061-T6 Al are displayed in Fig. 17. The relative tensile strength σ_{br}, relative tensile elongation, ε_{br} and relative fracture elongation ε_{fr} do not change with the increase of ultrasonic amplitude. During the conventional tensile test, the relative tensile strength σ_{br} = 45.7 MPa, relative tensile elongation ε_{br} = 6.7%, and relative fracture elongation ε_{fr} = 12%. When the ultrasonic amplitude increases to 8.7 μm, the σ_{br}, ε_{br}, and ε_{fr} are 43.7 MPa, 6.2%, and 11.9%, respectively. It can be stated that the ultrasonic amplitude does not change the final tensile properties of 6061-T6 Al with the range of 0–8.7 μm.

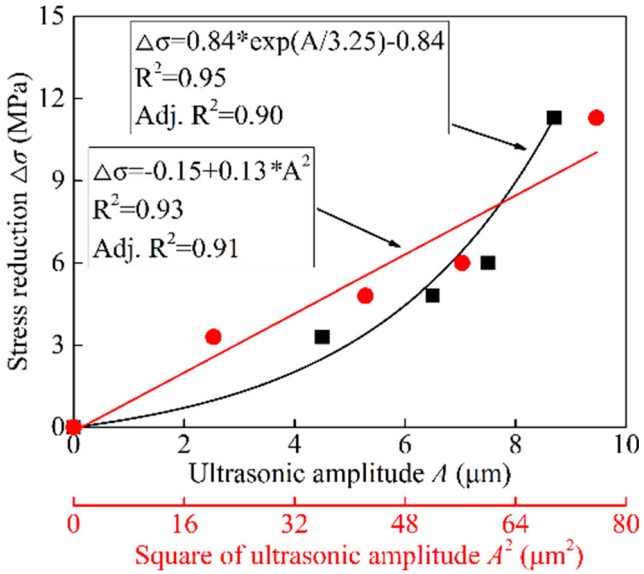

Fig. 15 Relationship between stress reduction and ultrasonic amplitude

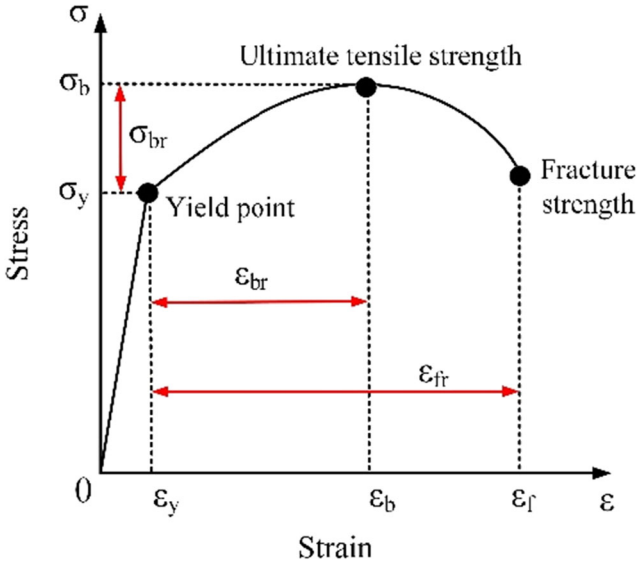

Fig. 16 Concept of σ_{br}, ε_{br}, and ε_{fr}

4.4 The Effect of ultrasonic vibration on the fracture morphology

Figure 18 depicts the fracture surface and its micromorphology of 6061-T6 Al specimen under different tensile conditions. The macroscopical fracture surface of 6061-T6 Al was the typical ductile fracture, which is accompanied by a cone cup-shaped fracture and necking. The micromorphology of the fracture surface demonstrates that the equiaxed dimples and micro-voids with different sizes exist. As can be seen from Fig. 18 a–f, when the ultrasonic vibration is applied considering the different deformation processes, duration time, and ultrasonic amplitudes, there is no big difference between the ultrasonic tensile and conventional tensile about the micromorphology of the fracture surface. The above results further indicate that the ultrasonic vibration has no permanent effect on the 6061-T6 Al during the tensile test.

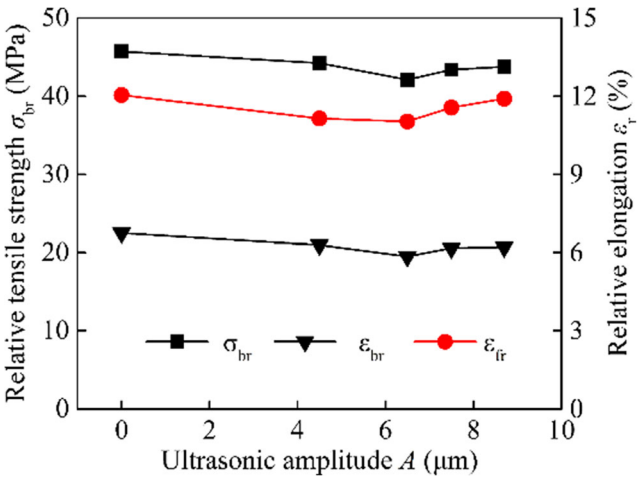

Fig. 17 The effect of ultrasonic amplitude on σ_{br}, ε_{br}, and ε_{fr}

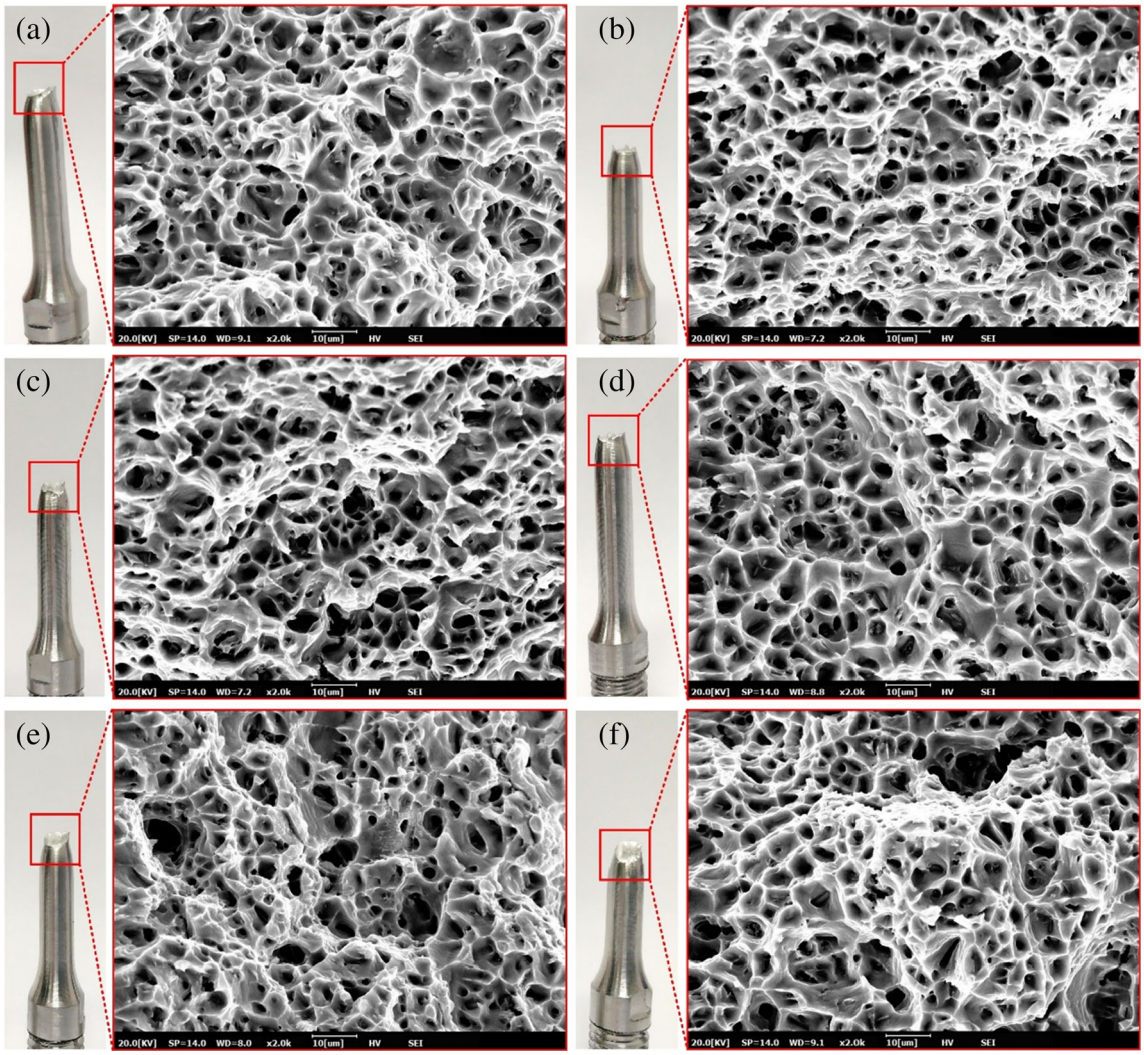

Fig. 18 Fracture morphology of 6061-T6 Al under the different tensile conditions: **a** test no. 1, **b** test no. 2, **c** test no. 3, **d** test no. 4, **e** test no. 5, and **f** test no. 8

5 Conclusions

(1) Based on the method of segmented resonance design, the ultrasonic vibration tensile device is developed. The error of resonance frequency between the designed value and the measured value is 3.3%, and the ultrasonic vibration amplitude of 8.7 μm can be achieved.

(2) Ultrasonic vibration is superimposed to 6061-T6 Al specimen during the tensile process. In the elastic deformation stage, ultrasonic vibration reduces the stress required for the elastic deformation of the material; however, it does not change Young's modulus. In the yield deformation stage, the yield strength of the material is reduced. In the plastic deformation stage, the ultrasonic vibration reduces the stress required for the plastic deformation, while it does not change the strain hardening rate of the material.

(3) Acoustic softening is observed and independent of the duration time of ultrasonic vibration when ultrasonic vibration is applied. The stress reduction is proportional to the square of ultrasonic vibration amplitude, which further indicates that the ultrasonic softening is attributed to the changed dislocation of 6061-T6 Al material.

(4) There is no residual effect after stopping the ultrasonic vibration during the tensile process. Comparing the tensile mechanical properties and fracture morphology, it can be concluded that ultrasonic vibration has no permanent effect on the final tensile behavior of the 6061-T6 Al.

Author Contribution Bangfu Wu conceived the analysis and wrote the manuscript. Yang Cao collected the data and revised the manuscript. Junshuai Zhao performed the experiment. Wenfeng Ding provided supervision on experimentation and manuscript preparation.

Funding This work was financially supported by the National Natural Science Foundation of China (Nos. 51921003 and 51775275), National Key Laboratory of Science and Technology on Helicopter Transmission (Nanjing University of Aeronautics and Astronautics) (No. HTL-A-20G01), and Six Talents Summit Project in Jiangsu Province (No. JXQC-002).

Data availability All data generated or analyzed during this study are included in the present article.

Declarations

Ethics approval The article follows the guidelines of the Committee on Publication Ethics (COPE) and involves no studies on human or animal subjects.

Consent to participate Not applicable.

Consent to publish Not applicable.

Competing interests The authors declare no competing interests.

References

1. Blaha F, Langenecker B (1955) Dehnung von zink- kristallen unter ultraschalleinwirkung. Naturwissenschaften 42(20):556–567
2. Bagherzadeh S, Abrinia K, Liu YF, Han QY (2017) The effect of combining high-intensity ultrasonic vibration with ECAE process on the process parameters and mechanical properties and microstructure of aluminum 1050. Int J Adv Manuf Technol 88(1-4): 229–240
3. Lou Y, Liu X, He JS, Long M (2018) Ultrasonic-assisted extrusion of ZK60 Mg alloy micro-pins at room temperature. Ultrasonics 83: 194–202
4. Yang CH, Shan XB, Xie T (2016) Titanium wire drawing with longitudinal-torsional composite ultrasonic vibration. Int J Adv Manuf Technol 83(1-4):645–655
5. Liu S, Shan XB, Guo K, Yang YC, Xie T (2018) Experimental study on titanium wire drawing with ultrasonic vibration. Ultrasonics 83:60–67
6. Hung JC, Hung CH (2005) The influence of ultrasonic-vibration on hot upsetting of aluminum alloy. Ultrasonics 43(8):692–698
7. Cao Y, Zhu YJ, Li HN, Wang CX, Su HH, Yin Z, Ding WF (2020) Development and performance of a novel ultrasonic vibration plate sonotrode for grinding. J Manuf Process 57:174–186
8. Cao Y, Zhu YJ, Ding WF, Qiu YT, Wang LF, Xu JH (2021) Vibration coupling effects and machining behavior of ultrasonic vibration plate device for creep-feed grinding of Inconel 718 nickel-based superalloy. Chin J Aeronaut. https://doi.org/10.1016/j.cja.2020.12.039 (Published online)
9. Fartashvand V, Abdullah A, Sadough Vanini SA (2017) Investigation of Ti-6Al-4V alloy acoustic softening. Ultrason Sonochem 38:744–749
10. Rusinko A (2011) Analytical description of ultrasonic hardening and softening. Ultrasonics 51(6):709–714
11. Hu J, Shimizu T, Yang M (2018) Investigation on ultrasonic volume effects: stress superposition, acoustic softening and dynamic impact. Ultrason Sonochem 48:240–248
12. Fartashvand V, Abdullah A, Sadough Vanini SA (2017) Effects of high power ultrasonic vibration on the cold compaction of titanium. Ultrason Sonochem 36:155–161
13. Cao MY, Hu H, Jia XD, Tian CC, Han XB (2020) Mechanism of ultrasonic vibration assisted upsetting of 6061 aluminum alloy. J Manuf Process 59:690–697
14. Xie ZD, Guan YJ, Zhu LH, Zhai JQ, Lin J, Yu XH (2018) Investigations on the surface effect of ultrasonic vibration-assisted 6063 aluminum alloy ring upsetting. Int J Adv Manuf Technol 96(9-12):4407–4421
15. Daud Y, Lucas M, Huang ZH (2007) Modelling the effects of superimposed ultrasonic vibrations on tension and compression tests of aluminum. J Mater Process Technol 186(1-3):179–190
16. Zhong CK (2016) Research of high-frequency vibration assisted aluminum alloy plastic forming. Shan Dong University (In Chinese)
17. Gu XM (2015) The performance testing of sheet metal ultrasound micro-tensile. Shen Zhen University (In Chinese)
18. Gao TJ, Liu XJ, Yu K, Qi L, Wang S (2019) Effect of ultrasonic vibration on tensile properties of TC1 titanium alloy sheet. Rare Metal Mater Eng 48(1):286–292
19. Wen T, Wei L, Chen X, Pei CL (2011) Effects of ultrasonic vibration on plastic deformation of AZ31 during the tensile process. Int J Miner Metall Mater 18(1):70–76
20. Dutta RK, Petrov RH, Delhez R, Hermans MJM, Richardosn IM, Bottger AJ (2013) The effect of tensile deformation by in situ ultrasonic treatment on the microstructure of low-carbon steel. Acta Mater 61(5):1592–1602
21. Jiang SS, Jia Y, Zhang HB, Du ZH, Lu Z, Zhang KF, He YS, Wang RZ (2017) Plastic deformation behavior of Ti foil under ultrasonic vibration in tension. J Mater Eng Perform 26(4):1769–1775
22. Xiang DH, Zhang ZM, Wu BF, Feng HR, Shi ZL, Zhao B (2020) Effect of ultrasonic vibration tensile on the mechanical properties of high-volume fraction SiCp/Al composite. Int J Precis Eng Manuf 21:2051–2066
23. Wang CJ, Zhang WW, Cheng LD, Zhu HQ, Wang XW, Han HB, He HD, Hua RS (2020) Investigation on microsheet metal deformation behaviors in ultrasonic-vibration-assisted uniaxial tension with aluminum alloy 5052. Materials 13(3):637
24. Mao Q, Coutris N, Rack H, Fadel G, Gibert J (2020) Investigating ultrasound-induced acoustic softening in aluminum and its alloys. Ultrasonics 102:106005
25. Lin ZM (1987) Principle and design of ultrasonic horn. Science press, Bei Jing (In Chinese)
26. Green CH (2000) Stress amplitude analysis in a generalized ultrasonic fatigue dumbbell specimen. J Phys D Appl Phys 24(3):469–477
27. Green CH (1979) Radius optimization in an ultrasonic specimen with a circular gauge profile. J Phys D Appl Phys 12(7):1191–1194
28. Han GC, Li K, Peng Z, Jin JS, Sun M, Wang XY (2017) A new porous block sonotrode for ultrasonic assisted micro plastic forming. Int J Adv Manuf Technol 89(5-8):2193–2202
29. Shimamura Y, Narita K, Ishii H, Tohgo K, Fujii T, Yagasaki T, Harada M (2014) Fatigue properties of carburized alloy steel in very high cycle regime under torsional loading. Int J Fatigue 60:57–62
30. Costa P, Vieira M, Reis L, Ribeiro A, Freitas MD (2017) New specimen and horn design for combined tension and torsion ultrasonic fatigue testing in the very high cycle fatigue regime. Int J Fatigue 103:248–257
31. Huang H, Pequegnat A, Chang BH, Mayer M, Du D, Zhou Y (2009) Influence of superimposed ultrasound on deformability of Cu. J Appl Phys 106(11):1144–1198
32. Langenecker B (1966) Ultrasonic treatment of specimens in the electron microscope. Rev Sci Instrum 37(1):103–106
33. Zhang YD (1995) Ultrasonic machining and its application. National Defense Industry Press, Bei Jing (In Chinese)